ChemPubSoc Europe

DOI: 10.1002/batt.201800150

BATTERIES & SUPERCAPS
Articles

Modelling Coupled Ion Motion in Electrolyte Solutions for Lithium-Sulfur Batteries

Silvio Osella[+],[a, c] Andrea Minoia[+],[a] Claudio Quarti,[a] Jérôme Cornil,[a] Roberto Lazzaroni,[a] Anne-Lise Goffin,[b] Maxime Guillaume,[b] and David Beljonne*[a]

We model coupled ion transport in representative electrolyte solutions for Li–S batteries by applying molecular dynamic (MD) simulations on systems of increasing complexity, namely going from solutions of the Li_2S_4 salt in pure tetraethylene glycol dimethyl ether (TEGDME) and 1,3-dioxolane (DOL) solvents, to Li_2S_4 in solvent mixtures, and finally incorporating lithium bis (trifluoromethanesulfonyl)imide (LiTFSI) as a reservoir of Li-ions. While the motion of Li_2S_4 salt in DOL is predominantly vehicular, it is governed by a hopping regime in the more viscous TEGDME solvent. Most importantly, when the two salts are mixed, the presence of the TFSI anions does not slow down the diffusion of the polysulfide anion.

1. Introduction

The increasing consumption of fossil fuels has raised much interest for alternative energy sources and storage strategies over the last decades. Among these, lithium batteries are particularly attractive because of their versatility, ease of production and high performances.[1,2] In particular, a high theoretical gravimetric capacity of 1675 mAh g^{-1} is anticipated for a lithium metal anode coupled with a sulfur cathode,[3-5] whereas the highest capacity obtained is 275 mAh g^{-1} for state-of-the-art Li-ion batteries (such as $LiCoO_2$-Graphite).[6] Li–S batteries are expected to deliver a theoretical energy density of 2600 Wh kg^{-1} assuming a complete reaction to Li_2S, which is much higher than the values reported for state-of-the-art Li-ion batteries today, not exceeding 500 Wh kg^{-1}.[7-12] In addition, sulfur is abundant in nature, inexpensive and environmentally friendly, implying that Li–S batteries should be cheaper than the currently available Li-ion batteries based on transition metals. In the last ten years, many research efforts have been dedicated to the development of Li–S batteries, with the aim of identifying and overcoming the limiting factors that prevent their high theoretical efficiency to be turned into practice.[13-15] In particular, the focus was on the development of better cathodes[16-20] and in the understanding of the complex redox mechanisms governing the sulfur chemistry.[21-24] In fact, multiple polysulfide (PS) species are present in working batteries, ranging from the soluble Li_2S_8–Li_2S_4 to the insoluble Li_2S_2 and Li_2S species, with all of them playing an important role in the function of the cell.[25,26]

Despite those research efforts, many open questions remain. In particular, the solubilisation of the lithium polysulfide (LiPS) species in ether solvents containing the electrolyte leads to the destructuration of the cathode.[27] In addition, the diffusion of the LiPS and their conversion into a Li_2S precipitate results in the formation of solid deposits that passivate the electrodes, leading to the chemical corrosion of the lithium anode.[28] Moreover, the long LiPS chains are reduced on the Li anode surface in shorter LiPS chains that diffuse to the cathode where they re-oxidize (in the charging process), leading to 'LiPS shuttle' processes that cause self-discharge and poor charging efficiency. This shuttle effect is supposed to be partially controlled by the diffusion properties of the LiPS species in the electrolyte, the ion motions competing with the kinetics of the oxidation and reduction at the electrodes. Therefore, strategies to block or slow down the polysulfide species in the electrolyte are highly desirable in order to decrease this shuttle effect. This parasitic effect causes limited cycle stability of the LiS batteries, preventing the full recovery of the battery initial capacity and leading to infinite charge-discharge profiles at low voltage.[29,30]

In order to get a better understanding of the ion transport mechanisms at the heart of the battery operation and identify strategies to hamper (or at least reduce) the shuttle effect, a comprehensive and quantitative study of the liquid electrolyte phase is definitively required. The electrolyte used for working Li–S batteries is usually made of a mixture of organic solvents and salts. The electrolyte must be chemically stable in the presence of PS, have low toxicity, low volatility, low flammability and ensure high Li conductivity, which in turn leads to fast Li-ion transport.[29] To fulfil all these requirements, mixtures of complementary solvents, namely ether-based solvents such as tetraethylene glycol dimethyl ether (TEGDME) and 1,3-dioxo-

[a] *Dr. S. Osella,[+] Dr. A. Minoia,[+] Dr. C. Quarti, Prof. J. Cornil, Prof. R. Lazzaroni, Prof. D. Beljonne*
Laboratory for Chemistry of Novel Materials
University of Mons
Place du Parc 20, B-7000 Mons, Belgium
E-mail: david.beljonne@umons.ac.be
[b] *Dr. A.-L. Goffin, Dr. M. Guillaume*
Resarch & Innovation
SOLVAY SA
rue de Ransbeek 310, 1120 Brussels, Belgium
[c] *Dr. S. Osella[+]*
Current address: Chemical and Biological Systems Simulation Lab
Center of New Technologies
University of Warsaw
Banacha 2 C, 02-097 Warsaw, Poland
E-mail: s.osella@cent.uw.edu.pl
[+] *These authors contributed equally to the work.*

lane (DOL), have been widely used.[5,31] DOL is beneficial in TEGDME-DOL binary mixtures as it abates the effective solvent phase viscosity and forms a protective layer over the Li anode,[32] while TEGDME efficiently solubilizes and dissociates Li salts and has high thermal stability.[33] An additional lithium salt is also added to the solvent mixture to bring additional useful features, including a reservoir of Li-ions, negligible volatility, low flammability, high thermal stability, good conductivity and a wide electrochemical potential window.[29,34,35] One of the most common salt used in Li–S batteries is lithium bis(trifluoromethanesulfonyl)imide (LiTFSI). Since the TFSI anion has a low binding affinity with the Li cation, it should enhance the ion dissociation and improve the conductivity of the battery.[36] A properly tuned ratio of Li salt versus solvent concentration has been suggested to promote efficient Li diffusion and limited shuttle transport of the PS dianions.[14]

Summarizing, boosting the performances of Li–S batteries requires maximizing the diffusion coefficient of the Li cations while simultaneously suppressing PS transport. On a more fundamental vein, the ions present in the liquid electrolyte can diffuse with two different mechanisms: the first one, referred to as vehicular mechanism, consists in the motion of the lithium cations together with their coordination shell (including counter-ions and solvent molecules); the second one, called hopping or structure diffusion mechanism, is present when Li-ions exchange the anions and/or solvent molecules in their first coordination shell. Hopping is expected to be more favourable for decoupling the motion of Li and sulfide ions in the batteries.

In this work, we use classical force field molecular dynamics (MD) simulations to study the diffusion of ions present in compositions of liquid bulk electrolytes used for Li–S battery applications, ranging from simple pure solvents to more complex mixed electrolytes. The mechanistic aspects of ion transport are identified, which can hopefully guide the design of efficient electrolytes meeting the stringent requirements for usage in Li–S batteries.

2. Methodology

To gain a thorough understanding of the mechanistic aspects of ion transport in electrolytes, we have considered models of increasing complexity. The chemical structure of all investigated species is reported in Figure 1. Note in particular that we choose to focus on Li_2S_4 as a representative case study for PS species.

We start our analysis with Li_2S_4 based electrolytes, namely Li_2S_4:DOL, Li_2S_4:TEGDME and Li_2S_4:DOL:TEGDME (in 1:1 DOL:TEGDME ratio). Next, the effect of adding LiTFSI to Li_2S_4:DOL:TEGDME is considered, thereby closely mimicking the actual conditions typically encountered in Li–S batteries. The theoretical approach used relies on a modified version of the OPLS-AA Force Field,[37] whose parameterization has been extended to properly account for both the solvents and salts considered here and validated against experimental data in the literature (see Supporting Information for more details).

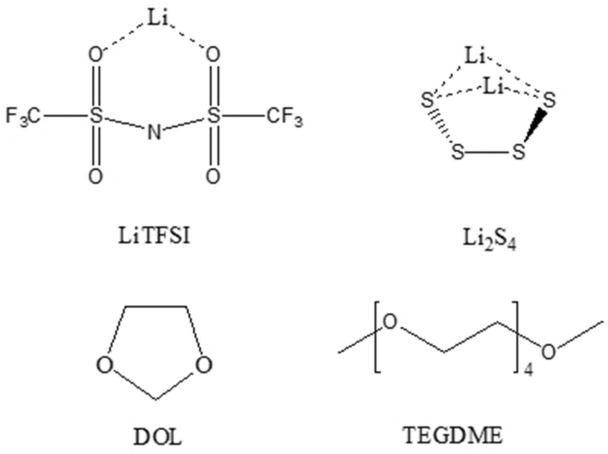

Figure 1. Chemical structure of the electrolyte components (LiTFSI and Li_2S_4 salts; DOL and TEGDME solvents) investigated here.

2.1. Force-Field Molecular Dynamics Simulations

2.1.1. Optimization of the Force Field Parameters for S_n^{2-} and Li_2S_n Polysulfide Species

A challenge for modelling actual battery operations is to deal with different Li_2S_n species in the solvent environment, all possibly interacting with each other and displaying different behaviours (i.e., the shortest molecules are insoluble). Here, for the sake of simplicity, we focused on one of the predominant soluble species, namely Li_2S_4.[22] We expect that the conclusions derived from these investigations can be generalized to the other soluble polysulfides. We selected the standard OPLS force field (FF) because of its reliability in the description of liquid systems and its validation for many different solvent molecules.[38-40] To properly model the Li_2S_4 molecules, the OPLS FF has been extended by adding new parameters to describe the torsions in the PS chain backbone. Besides, accurate atomic charges (as obtained from correlated quantum-chemical calculations) have been used to properly account for the electrostatic interactions between the different ionic species in the electrolytes.

The details for the PS torsion parameterisation and optimized values of the new force parameters are reported in the Supporting Information. All MD simulations were performed with the highly efficient molecular modeling package GROMACS 4.5.5.[41]

In order to derive all missing FF parameters needed to describe PS molecules, we parameterized the S_4H_2 neutral molecule, in vacuum, against ab initio post Hartree-Fock MP2 calculations, since it is the shortest molecule possessing all characteristic internal degrees of freedom of longer PS chains (i.e., stretching, bending and torsions between sulfur atoms). Because the torsional angles in the OPLS FF are affected by the 1–4 electrostatic and vdW interactions, we used atomic charges calculated via the Electrostatic Potential (ESP) method, using the Dunning's TZVP basis set,[42] as implemented in the Gaussian09 program.[43]

Next, the geometry of the S_4^{2-} ion was optimized at the MP2 level of theory and the parameterization procedure for the torsion was repeated; interestingly, such a parameterization turned out to be transferable, so that, as long as the proper MP2/ESP charges are used, the torsion and other bonding parameters derived for S_4^{2-} readily apply to longer (shorter) PS.

Finally, we optimized the geometry of a Li_2S_4 complex at the MP2 level of theory, with the TZVP basis set. We imposed a nominal charge of $+1$ $|e|$ on the Li^+ ions, while for S_4^{2-} we used the distribution of ESP partial charges obtained from the MP2 optimization of the salt in vacuum.

2.1.2. Parameterization of the Solvents

The original OPLS FF parameters used for the simulation of DOL were taken from literature.[44] Because no OPLS parameters were found in the literature for TEGDME, we used the standard OPLS parameters defined for a similar, but shorter, member of the glycol family, namely diethylene glycol dimethyl ether. The ESP charges from MP2 calculations were used as atomic charges for both solvent molecules (the parameters and ESP charges used are reported in the Supporting Information).[39]

Pure solvents were modelled and equilibrated at ambient temperature and pressure by using a common procedure consisting in a series of MD simulations each at different pressure and temperature.[44] The procedure is detailed in the Supporting Information. For both equilibration (NPT ensemble) and production (NVT ensemble) simulations, the Particle Mesh Ewald (PME) algorithm[45] was applied to describe the Coulomb interactions, with a switched cut-off of 1.1 nm. A cut-off of 1.1 nm was used for the LJ interactions. For the production simulations, we adopted the Nose-Hoover algorithm for temperature coupling, with a coupling time constant of 1 ps. Constant pressure calculations were performed on the basis of the Parrinello-Rahman algorithm, with compressibility set to $5 \cdot 10^{-5}$ bar^{-1} and a time constant of 5 ps.

Because OPLS is not a polarisable FF, the description of the electrostatics in the solvent phase needs to be carefully addressed, since it should reflect the interaction between the static atomic charges (as prevailing in the isolated units) as well as the charge redistribution induced by the electronic polarization effects. Simply considering $\varepsilon = 1$ in the Coulomb term would neglect the dynamic (induction) polarization effects, whereas including the static dielectric constant of the solvent would roughly amount to counting twice the static interactions. Recent theoretical works[46,47] have demonstrated that the electronic polarization in ionic liquids can be accounted for by scaling the Coulomb interactions by a factor $1-1/\varepsilon_{el}$, where ε_{el} is the (fast/optical) electronic dielectric constant of the medium, which can be determined by experimental measures of the refractive index as $\varepsilon_{el} = n^2$.[48] From the refractive indices of 1.3979 for DOL and 1.4307 for TEGDME at room temperature,[49] we obtain ε_{el} values of 1.18 for DOL and 1.19 for TEGDME. With this in mind, all MD simulations in this work have been performed by screening the Coulomb interactions by an effective dielectric constant of 2, to implicitly account for the electronic polarization effects. The total MD simulation time for DOL was 40 ns : 20 ns for equilibration and 20 ns for production runs. The MD calculations were considered converged when the absolute drift in total energy becomes lower than 50 $J\,mol^{-1}\,ns^{-1}$. Since TEGDME is highly viscous, molecular mobility at room temperature is limited; an annealing procedure (see Supporting Information) was therefore performed to reach equilibrium within a reasonable MD duration.

To validate the accuracy of the FF parameterization for the pure solvents, the density and diffusion coefficient were extracted from the MD production runs and compared with experimental data measured by pulse-gradient spin-echo NMR (PFG-NMR), as reported in literature.[50-52] The calculated densities for DOL and TEGDME (0.970 and 0.978 g/cm^3) are slightly underestimated (by 8% and 3%, respectively) with respect to the corresponding experimental values (1.06 g/cm^3 and 1.0 g/cm^3); differences below 10% are usually considered as acceptable.[44] The diffusion coefficient has been evaluated with the Einstein relation:

$$D_i = \lim_{t\to\infty} D_i^{app}(t) = \lim_{t\to\infty} \frac{\langle MSD_i(t)\rangle}{6t} \quad (1)$$

where $MSD_i(t)$ is the mean square displacement of the molecular center-of-mass averaged over the simulation time t and $D_i^{app}(t)$ is the time-dependent apparent diffusion coefficient. The predicted room temperature (300 K) diffusion coefficient is 18.1 10^{-10} m^2/s for DOL and 1.7 10^{-10} m^2/s for TEGDME, which compare well with the experimental values of 23.5 and 3.25 10^{-10} m^2/s, respectively. The larger D values predicted and measured for DOL versus TEGDME are consistent with the relative viscosity η of the two solvents (0.59 and 4.1 mPa·s, respectively) and in line with the Stokes-Einstein relation (with D inversely proportional to η).

2.1.3. Parameterization of LiTFSI Salt

The FF parameters for the TFSI anion were taken from literature,[53] with the charges calculated at the MP2/ESP level as in the polysulfide case. For the sake of consistency with the PS calculations, we also adopted the nominal $+1|e|$ charge for Li cations in LiTFSI. The C–S–N–S torsion potential was parameterized with the new set of ab initio partial charges, see Figure S5 in Supporting Information. In agreement with the MP2 calculations, the bi-dentate structure, in which the Li-ions are interacting with two oxygen atoms, is found to be the most stable. The validity of the force-field description of the salts has been further checked by running ab initio Born-Oppenheimer Molecular Dynamics (BO-MD) simulations, in which polarization effects are inherently considered. The structural analysis reported in the Supporting Information shows that the force field description is robust against the ab initio results for both Li_2S_4 and LiTFSI salts.

2.1.4. Modelling Workflow

The modelling and characterisation of the different models presented in this work were done in multiple steps. We began creating a cubic periodic box filled with a solvent to salt ratio of 20:1. Since the solvent phase is modelled with roughly the same number of solvent molecules (~800), the size for the modelled periodic box for DOL and TEGDME solutions is about $4\times4\times4\ nm^3$ and about $7\times7\times7\ nm^3$, respectively. All systems have been prepared using the same protocol. First, the classic conjugate gradient algorithm was used to minimise the energy of the models after construction. Next we run a 12 ns long molecular dynamics simulation in the NPT ensemble at 300 K and 1 atm to equilibrate the system in terms of energy and density. During the equilibration phase, the pressure and temperature were controlled with the Parrinello-Rahman barostat (1 bar, with a time constant of 5 ps and compressibility $4.5\times10^{-5}\ bar^{-1}$) and Nose-Hoover thermostat (300 K and time constant of 0.5 ps). After equilibration, a production run consisting in a 20 ns-long MD simulation was performed in the NVT ensemble at 300 K, and the relevant data extracted from the trajectories. In this production phase, the temperature was controlled by the Nose-Hoover thermostat. The time step for the integration of the equation of motion was kept to 2 fs with the LINCS algorithm. The Particle Mesh Ewald (PME) method was used to compute Coulomb and van der Waals interactions within a 1.1 nm cut-off, together with an effective dielectric constant of 2, to implicitly account for the electronic polarization effects and screen the Coulomb interactions.

2.2. Transport Properties

In order to assess how the salts interact with the solvents and their degree of aggregation or dissociation, we performed a structural analysis by means of radial distribution functions (RDF) and cumulative radial distribution functions (CRDF).

Because ionic conductivity is related to the ionic mobility in the electrolyte, the mobility for all molecular species present in the electrolytes has been calculated with Equation 1. The degree of uncorrelated ion motion in the electrolyte, α, has also been computed for the different systems. This quantity is defined as the ratio of the actual total ionic conductivity in the system, λ, and the ideal ionic conductivity calculated as if each ion in the system was diffusing independently from the others (λ_{uncorr}):

$$\alpha = \frac{\lambda}{\lambda_{uncorr}} = \lim_{t\to\infty}\alpha(t) = \lim_{t\to\infty}\frac{\lambda^{app}(t)}{\lambda^{app}_{uncorr}(t)} \tag{2}$$

$$\lambda = \lim_{t\to\infty}\lambda^{app}(t) = \lim_{t\to\infty}\frac{e^2}{6tVk_bT}\sum_{ij}^{N} z_i z_j \langle [R_i(t)-R_i(0)]\left[R_j(t)-R_j(0)\right]\rangle \tag{3}$$

where e is the electron charge, V the volume of the simulation box, k_b the Boltzmann constant, T the temperature, z_i the charge of ion i, N the total number of ions in the simulation box and $R_i(t)$ the position of ion i at time t. The corresponding ionic conductivity assuming that ions move in a completely uncorrelated way writes:

$$\lambda^{app}_{uncorr}(t) = \lim_{t\to\infty}\lambda^{app}_{uncorr}(t) = \frac{e^2}{6tVk_bT}\sum_{i}^{N} z_i^2 \langle [R_i(t)-R_i(0)]^2\rangle \tag{4}$$

As a result, α denotes the degree of interaction between the ions; when $\alpha=0$, the ions move together in a pure vehicular mechanism, while for $\alpha=1$ the ions move in a pure hopping mechanism. It should be noted that the determination of α is considered to be accurate in the first 5% of the MD trajectory.[54]

3. Results and Discussion

In all MD simulations, we consider a solvent to salt ratio of 20:1 for the purpose of comparison with experimental data from the literature.[50] For each system, the solvent phase has been first equilibrated at ambient pressure and temperature. After equilibration, 20 to 40 ns-long production MD runs are conducted in the NVT ensemble. All structural and transport data presented are extracted from the production runs.

With the aim of providing a comprehensive picture for the electrolytes used in LiS batteries, we have investigated first Li_2S_4-based electrolytes and later examined how those properties are modified when LiTFSI is added to the medium.

3.1. Li_2S_4 in Pure Solvents

To test our methodology, we first study the simpler case of a single Li_2S_4 molecule in DOL. Figure 2A shows the RDF for the solvated molecule in the periodic simulation cell (a representative structure is reported in Figure 2B). The RDF shows a single peak at short distances and goes to zero beyond 4 Å, meaning that for larger distances, a Li^+ cation does not see any sulfur atom. While the long-range behaviour of the RDF gives information on the dispersion of the salts in the solution, the RDF at short range gives information about the radius of the coordination shell (taken to be the position of the minimum after the first peak). In this case, we have only one peak and the radius of the coordination cell is 3.75 Å. We would like to stress that Figure 2A refers to the radial distribution function for the interaction between Li^+ and S^- atoms for a single Li_2S_4 complex in DOL solvent. This has been performed as simple test for the methodology, namely to check the behaviour of a single Li_2S_4 complex dispersed in DOL. Having only one salt molecule in the model, the peak of the Li–S RDF shown in Figure 2A corresponds to the Li–S interaction within a salt molecule. The broadness of the peak is related to the molecular geometry, where mainly two Li–S bond lengths (of 2.3 and 2.8, respectively) can be identified. The CRDF in Figure 2C shows that, within the coordination shell, every Li^+ is interacting on average with the other Li^+ cation, 4 sulfur atoms and 2.4

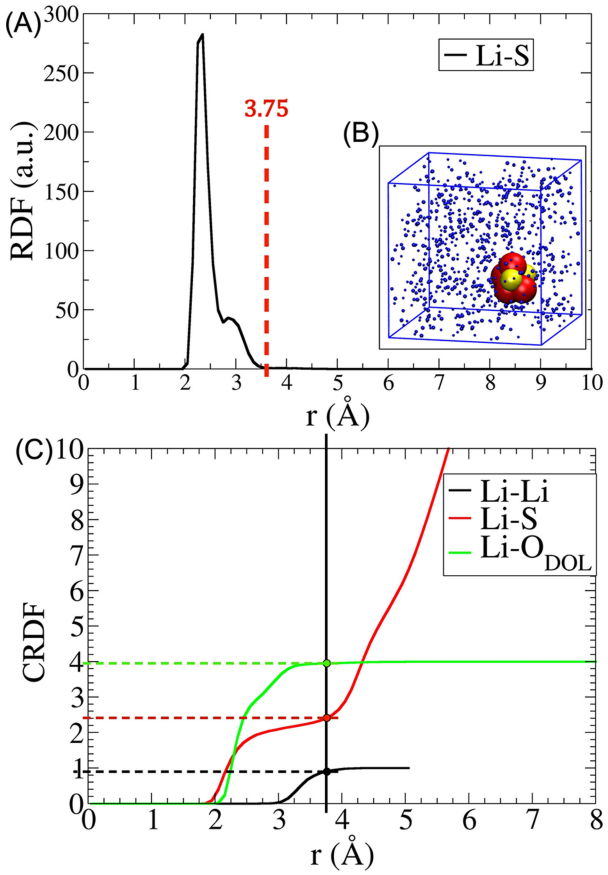

Figure 2. A) RDF for Li–S atoms for a single Li_2S_4 molecule in DOL. The red dashed line shows the size of the coordination shell. B) Final structure from the MD simulation (the solvent molecules are shown as small blue dots for the sake of clarity). C) CRDF for a single molecule of Li_2S_4in DOL. The vertical solid black line shows the size of the coordination shell. The circles and the horizontal dashed lines are used to highlight the values of the CRDFs distribution for the coordination cell.

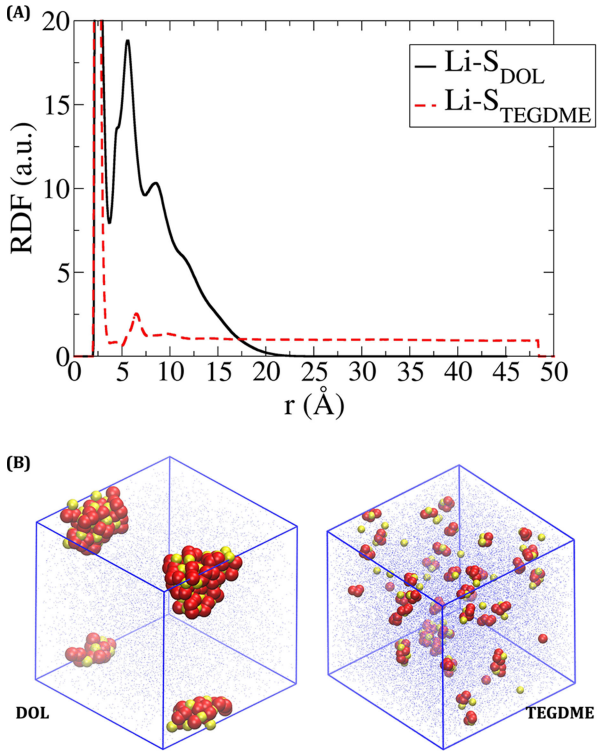

Figure 3. A) RDF distributions of Li–S in Li_2S_4–DOL (black) and Li_2S_4-TEGDME (red) for the 20:1 solvent-salt mixture. B) Final structures for the two electrolytes extracted from the MD simulations. The Li_2S_4 molecules are color coded in red (S) and yellow (Li) and the solvent molecules are shown as small blue dots for the sake of clarity.

Table 1. Radius and average composition of the Li^+ coordination shell for Li_2S_4 in DOL and TEGDME. For reference, the values obtained for a single Li_2S_4 molecule in DOL are also reported.

Solvent	Radius [Å]	#Li^+	#S	#$O_{solvent}$
Single Li_2S_4 in DOL	3.75	0.9	4	2.4
Li_2S_4 in DOL	3.65	1.5	6.8	0.5
Li_2S_4 in TEGDME	3.75	0.06	2.4	4

oxygen atoms from DOL molecules. Each cation thus interacts with the rest of the salt molecule; in other words, DOL does not promote the dissociation of the salt, as clearly seen in Figure 2B.

Next, we model Li_2S_4-DOL and Li_2S_4-TEGDME solutions in a 20:1 solvent to salt ratio, equilibrated at ambient temperature and pressure. The comparison between the Li–S RDFs in DOL and TEGDME (Figure 3A) shows a single peak in TEGDME and a broader distribution in DOL. When examining the situation at long range, the curve goes to zero in DOL, meaning that Li-ions do not see any sulfur atom located outside of a sphere with ~23 Å radius. This clearly indicates that all molecules aggregate in a single, large cluster. The behaviour is markedly different in TEGDME: the RDF converges to 1 beyond 12 Å, which is typical of a homogenous liquid solution and suggests that Li_2S_4 salt molecules are well dispersed in TEGDME. The final structures from the MD simulations in DOL and TEGDME (Figure 3B) support this interpretation.

The Li^+ coordination shells in DOL and TEGDME have a radius of 3.65 Å and 3.75 Å, respectively, and their compositions are reported in Table 1, together with that for a single salt molecule in DOL. CRDFs distributions are shown in Figure 4(A–B). The Li^+ coordination shell in DOL is slightly smaller than that of the single salt molecule because of the aggregation, but the composition shows that, on average, every cation interacts not only with its anion, but it is also partially interacting with another salt molecule. The interactions with the solvent molecules are very scarce, implying that most of the Li_2S_4 molecules are not in contact with the solvent, but are rather embedded in the aggregate. In strong contrast, the composition of the Li^+ coordination shell in TEGDME is dominated by solvent molecules, indicating that the salt is not only dispersed, but also at least partially dissociated.

From the RDF analysis, we can conclude that the capability of DOL to solvate, disperse and/or dissociate Li_2S_4 is rather poor, while TEGDME is a much more efficient solvent in that respect.

We next move to the calculation of transport properties of Li_2S_4 in the two solvents. In DOL, the diffusion coefficients for

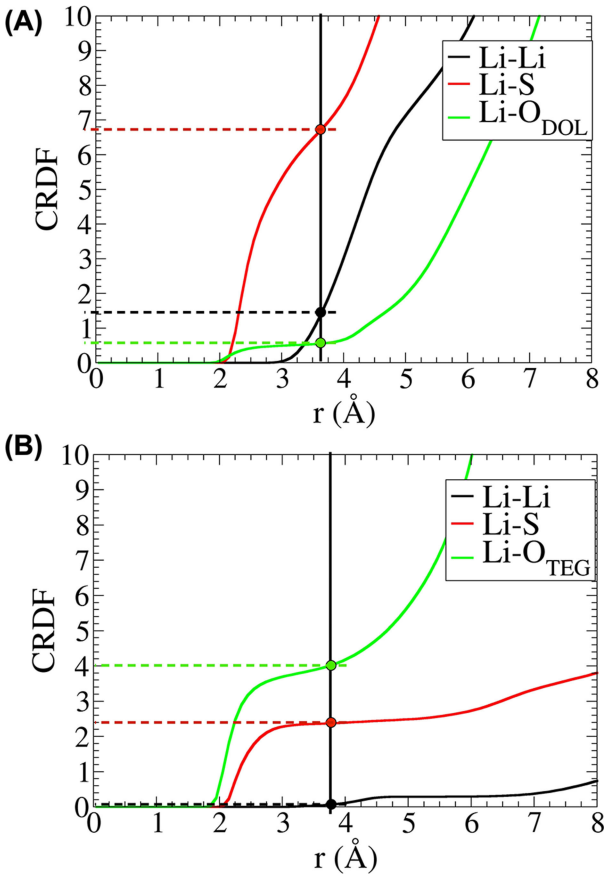

Figure 4. CRDF for Li_2S_4 in DOL (A) and in TEGDME (B). The vertical solid black line shows the size of the coordination shell. The colored dots and the horizontal dashed lines are used to highlight the values of the CRDFs distribution for the coordination cell.

3.2. Li_2S_4 in Mixed Solvents

To move a step closer to the composition of actual electrolytes in Li–S batteries, we have investigated a system in which Li_2S_4 has been placed into a homogenous mixture of the two solvents in a 1:1 ratio, maintaining the usual solvent to salt ratio of 20:1. The choice of the two solvents and their ratio has been made based on literature data showing that this composition yields improves ion conductivity with respect to the corresponding solutions in a single solvent.[4,55]

In Figure 5A, we compare the Li–S RDFs between the DOL, TEGDME and DOL:TEGDME electrolytes. The RDF analysis

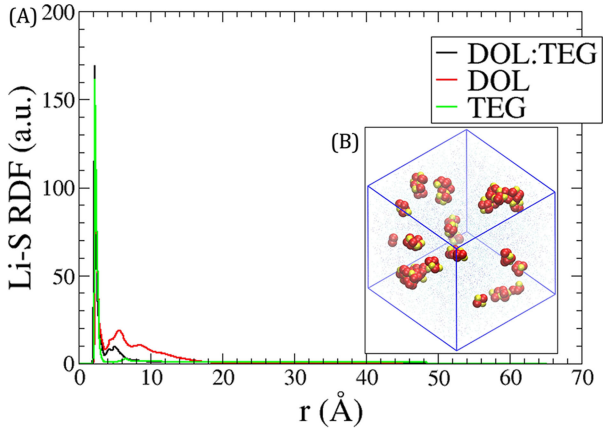

Figure 5. A) Comparison of Li–S RDF distribution for the three electrolytes. B) Final structure extracted from the MD simulations of the Li_2S_4:DOL:TEGDME electrolyte. The Li_2S_4 molecules are color coded in red (S) and yellow (Li). The solvent molecules are shown as small blue dots for the sake of clarity.

both Li^+ and S_4^{2-} ions are about 3×10^{-10} m^2/s, while in TEGDME the diffusion coefficients drop down to 0.5×10^{-10} m^2/s. For the sake of comparison, the diffusion coefficients for the DOL and TEGDME molecules are 28×10^{-10} m^2/s and 1.0×10^{-10} m^2/s, respectively. We would like to point out that the dispersion of the Li_2S_4 complexes in the two solvents is not directly related to their diffusion coefficients. The physical properties of the solvents should also be considered. In fact, the viscosity of TEGDME is much higher than for DOL, as reported in the Method section 2.1.2. This is the reason for the lower mobility in TEGDME, as also observed in experiments;[50–52] the lower mobility of the solvent molecules and ions in TEGDME is not surprising, as it is a more viscous solvent than DOL. It should be stressed that, being less viscous,[50] DOL should favour ion transport over TEGDME. In contrast, owing to the larger number of oxygen atoms, TEGDME is a better ion chelating agent.[29] The degree of uncorrelated ion motion, α, has been calculated in order to assess the mechanism for the ion transport of Li_2S_4 in the two media. In DOL, α is estimated to be 0.49, which suggests that ion motion occurs with a mixed vehicular and hopping mechanism implying exchanges of the counter-ions around a lithium atom within the aggregate; in TEGDME, the mechanism for ion transport has an increased hopping character, being characterized by $\alpha\sim0.61$.

indicates that the Li_2S_4:DOL:TEGDME electrolyte has a structure that is intermediate between those of Li_2S_4:DOL and Li_2S_4:TEGDME. At short range, the RDF resembles that of Li_2S_4:DOL (i.e., strong peaks below 10 Å), which suggests a certain degree of salt aggregation. However, at long range, i.e., for distances larger than 12 Å, the RDF goes to 1 as in the case of Li_2S_4:TEGDME, indicating homogenous dispersion in the solution. In other words, the solution is expected to be made of small clusters of salt molecules quite homogeneously distributed in the solvent, as can be seen from the final snapshot of the MD simulations (Figure 5B). This is further confirmed by the analysis of the coordination behaviour: the composition of the Li^+ coordination shell is very similar to that in DOL. The radius is 3.65 Å and each cation interacts with 1.5 Li^+, 4.8 S, 0 O_{DOL} and 2 O_{TEGDME} (CRDFs distributions are reported in Figure 6). This reinforces our previous findings that the presence of DOL favours the salt aggregation and that TEGDME instead stabilizes small Li_2S_4 clusters that are dispersed in the solution.

As in the previous systems, we have calculated the mobility of the different species and the degree of uncorrelated ion motion. The diffusion coefficients for both Li^+ and S_4^{2-} ions are about 0.5×10^{-10} m^2/s (i.e., very close to the values found in TEGDME), while the DOL and TEGDME solvents have diffusion

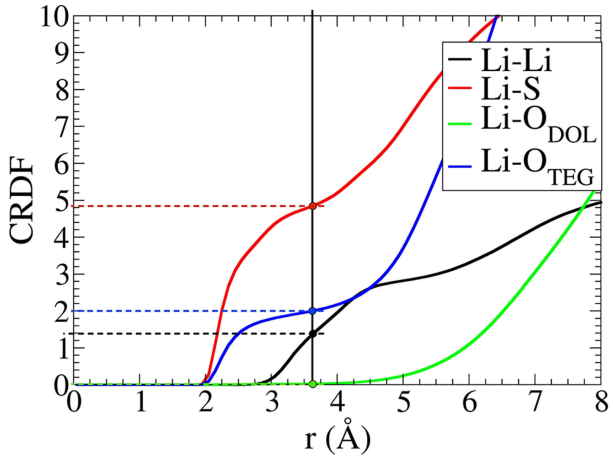

Figure 6. CRDF for Li_2S_4 in the mixture of DOL and TEGDME. The vertical solid black line shows the size of the coordination shell. The colored dots and the horizontal dashed lines are used to highlight the values of the CRDFs distribution for the coordination cell.

coefficients of about 5×10^{-10} m^2/s and 1.4×10^{-10} m^2/s, respectively (to be compared with the diffusion coefficients for the pure solvents of 28×10^{-10} m^2/s for DOL and 1.0×10^{-10} m^2/s for TEGDME). This indicates that the dynamics of solvent mixtures is ruled by TEGDME, which considerably slows down ion diffusion compared to pure DOL. The degree of uncorrelated ion motion, $\alpha = 0.53$, is intermediate between those calculated for the Li_2S_4:DOL and Li_2S_4:TEGDME electrolytes.

3.3. Adding LiTFSI to the Li_2S_4:DOL:TEGDME Electrolyte

Figure 7A shows the Li–S RDF, as calculated between all Li^+ cations present in the system and the sulfur atoms of all S_4^{2-} anions for the mixture of the two salts in the two solvents. The black curve in Figure 7A is the RDF for Li–S for which the cations originate from Li_2S_4 and the red curve corresponds to the cations originating from LiTFSI. The comparison between the two distributions reveals that there are interactions between Li^+ cations from LiTFSI and S_4^{2-} anions, pointing to a significant dissociation of LiTFSI in the electrolyte. At long range, the RDF again levels off at 1, consistent with the dispersion of the salt. Figure 7B indicates the presence of small molecular clusters comprising LiTFSI and Li_2S_4 molecules that are dispersed in the solution. Figure 7C displays the comparison between the RDFs for the Li^+ and the oxygen atoms of the solvent molecules and shows that there is a strong competition between the TEGMDE solvent and TFSI anions to capture the Li^+ cations, while very little interaction is found with DOL molecules. From the Li–S RDF, we determine the size of the coordination shell to be 3.85 Å. From the CRDF, a Li^+ cation interacts with 0 N_{TFSI}, 0 O_{DOL}, 3.75 O_{TEG}, 0.28 O_{TFSI} 1.83 S_{S4} and 1.01 S_{TFSI} within its coordination shell (CRDF distributions for this system are shown in Figure 8). By comparing the composition of the Li^+ coordination shell with that in the Li_2S_4:DOL:TEG electrolyte, the modelling suggests that the presence of LiTFSI helps to dissociate the salts and promotes the solvation of Li^+.

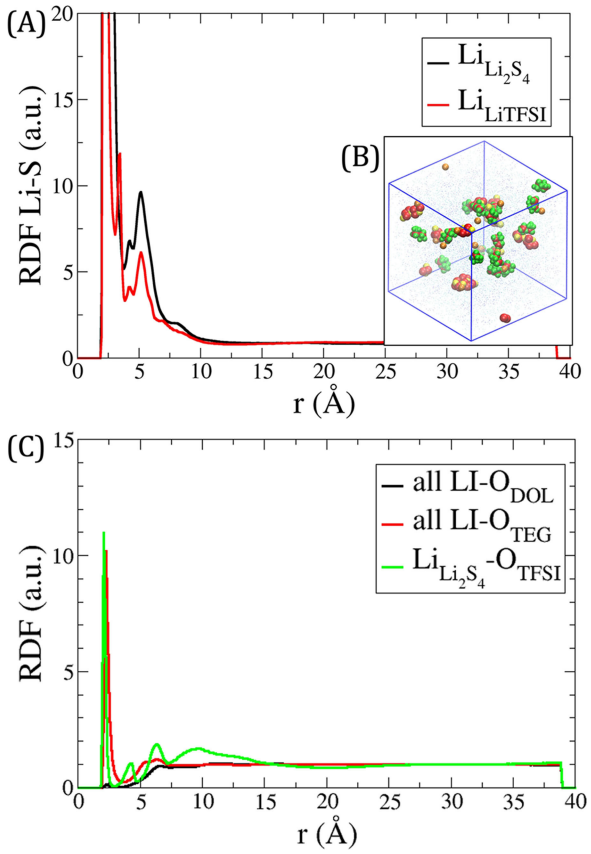

Figure 7. A) Li–S and C) Li–O RDF distributions in the LiTFSI:Li_2S_4:DOL:TEGDME system. B) Final structure extracted from the MD simulations. The Li_2S_4 molecules are color coded in red (S) and yellow (Li); the $TFSI^-$ anions are color coded in green and red (S) and the Li^+ cations in orange. The solvent molecules are shown as small blue dots for the sake of clarity.

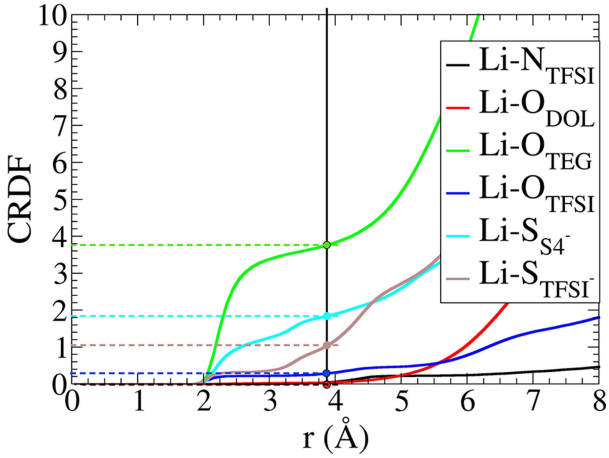

Figure 8. CRDF for the system where LiTFSI is added to Li_2S_4:DOL:TEGDME electrolyte. The vertical solid black line shows the size of the coordination shell. The colored dots and the horizontal dashed lines are used to highlight the values of the CRDFs distribution for the coordination cell.

The Li^+, S_4^{2-} and $TFSI^-$ ion mobilities are 0.7×10^{-10} m^2/s, 0.5×10^{-10} m^2/s and 1.0×10^{-10} m^2/s respectively. The mobility of the solvent molecules and S_4^{2-} anions are not affected by the LiTFSI salt, i.e., the values are the same as those calculated for the Li_2S_4:DOL:TEGDME electrolyte. The slight increase in the mobility of Li^+ when LiTFSI is present in the electrolyte (0.7×10^{-10} m^2/s vs 0.5×10^{-10} m^2/s) is expected to help decoupling the Li^+ versus S^{2-} motion. The degree of uncorrelated ion motion, α, has been calculated for pairs of ions, namely Li^+–S_4^{2-} and Li^+–$TFSI^-$. The ion motion for Li^+–S_4^{2-} has a mixed character ($\alpha=0.49$) while for Li^+–$TFSI^-$ ion pairs, the motion occurs clearly with a hopping mechanism ($\alpha=0.89$). As a result, the Li^+ cations sourced by LiTFSI diffuse faster, as they are less strongly bonded to the anion. Thus, it appears that LiTFSI has a very limited impact on the shuttle effect of LiPS, at least from a dynamical view point (since the diffusion is almost unaltered), but mainly acts as a reservoir of Li^+ cations while slightly improving their diffusion.

Table 2 summarizes the main findings from this study. It points to the need for a subtle interplay between the ability of the salts to dissociate and disperse in the solvent and the viscosity-dependent ion transport in the electrolytes. More specifically, our simulations show that: 1) the mixture of solvents with complementary characteristics (namely high chelation power and low viscosity) is crucial to ensure both dispersion and dissociation of the ions and ion transport; 2) the different behaviour of Li^+ in the two solvents reflects the different interaction energies of the Li^+ ions with the solvent, leading to the selectivity of Li-ion for one solvent. In fact, a good solvent should help in dispersing the Li-ions from the PS (the ideal solvent should be viscous to capture the S^{2-} anion) but at the same time should not interact too strongly to allow for a dynamic exchange of Li^+ ions without hampering their diffusion; 3) the analysis of the mixture of salts in the binary solvent environment strongly supports the finding that LiTFSI additives mostly act as a source of Li^+ cations without affecting the mobility of the PS anions and with limited impact on the (shuttle) diffusion mechanisms.

4. Conclusions

We have studied the electrolyte phase of LiS batteries by means of classic Molecular Dynamics simulations. A new and portable force field (FF) for the Li_2S_n salts has been developed and validated against ab-initio Born-Oppenheimer molecular dynamics calculations. This force field was used to model electrolytes of Li_2S_4 first in pure solvent environments (either DOL or TEGDME) and then in the solvent mixture. Finally, LiTFSI salt was added to the model in order to mimic a typical electrolyte used in working Li–S batteries.

The analysis of the transport properties, namely the diffusion coefficient and the degree of uncorrelated motion, allowed for the identification of the ion motion mechanism. We found that the ion motion mechanism for Li_2S_4 in pure DOL has mixed vehicular and hopping character, while in TEGDME a dominant hopping character prevails, probably owing to the improved degree of dissociation. This is borne out by the structural analysis of the TEGDME-based electrolyte. However, the high viscosity of that solvent strongly reduces ionic transport, thus calling for solvent mixtures. In a 1:1 DOL:TEGDME binary mixture, the Li_2S_4 ion motion has a mixed vehicular and hopping character. As a result, LiPS salts are better dispersed compared to pure DOL (which has no effect on the salt dissociation), yet ion motion is similar to that in the pure and highly viscous TEGDME solvent.

Finally, the addition of LiTFSI to the solvent mixture is predicted to slightly increase the mobility of Li-ions, while it hardly slows down the PS anion. In addition, the transport is now mixed (hopping) for the Li-ions originating from the PS (TFSI) salt, since the dissociation is not complete. Overall, it appears more likely from this study that the positive effect of LiTFSI additives in LiS batteries originates mostly from the increased number of mobile Li^+ cations, rather than shutting off PS anion diffusion in the electrolyte, especially at the beginning of the battery performance, where there is no presence of LiPS ions in the electrolyte. Yet, our study is not comprehensive of the whole mechanism which is much more complex. To the authors' knowledge, this is the first attempt to model the shuttle mechanism using MD simulations. From these simulations, the shuttle mechanism turns out to be much more complex than firstly hypothesized. With this first study, we shed light into a commonly accepted version of the mechanism, which is the decrease of the shuttle effect in presence of LiTFSI. However, further studies are clearly needed to include in the model the different species present in the electrolyte (from Li_2S to Li_2S_8), as well as the chemical reactions they are involved in, together with a more detailed analysis of the ion dynamics.

Table 2. Structural (aggregation or dispersion) and transport (diffusion coefficients and α value) properties for the different electrolytes.

Salt	Solvent	Structure	Diffusion Li^+ [10^{-10} m^2/s]	Diffusion A^- [10^{-10} m^2/s]	α	Diffusion Mechanism
Li_2S_4	DOL	Aggregation	2.8	2.8	0.49	Mixed
	TEGDME	Dispersion	0.5	0.5	0.61	Hopping
Li_2S_4	MIX	Clustering	0.5	0.5	0.53	Mixed
LiTFSI:Li_2S_4	MIX	Clustering	0.7	0.5 (S_4^{2-}) 1.0 ($TFSI^-$)	0.49 (Li_2S_4) 0.89 (LiTFSI)	Mixed Hopping

Acknowledgements

This study was supported by the Innoviris program of Région de Bruxelles-Capitale (project 2014-R-80, Solvay SA, the Science Policy Office of the Belgian Federal Government (IAP 7/5)) and FNRS (Consortium des Equipements de Calcul Intensif – CECI – program). D.B. and J.C. are research directors of FNRS.

Conflict of Interest

The authors declare no conflict of interest.

Keywords: diffusion coefficients · ion correlation · lithium-sulfur batteries · molecular dynamics · vehicular and hopping mechanisms

[1] X. Ji, L. F. Nazar, *J. Mater. Chem.* **2010**, *20*, 9821–9826.
[2] Y. V. Mikhaylik, J. R. Akridge, *J. Electrochem. Soc.* **2004**, *151*, A1969–A1976.
[3] J. Scheers, S. Fantini, P. Johansson, *J. Power Sources* **2014**, *255*, 204–218.
[4] L. Chen, L. L. Shaw, *J. Power Sources* **2014**, *267*, 770–783.
[5] S. S. Zhang, *J. Power Sources* **2013**, *231*, 153–162.
[6] A. Rosenman, E. Markevich, G. Salitra, D. Aurbach, A. Garsuch, F. F. Chesneau, *Adv. Energy Mater.* **2015**, *5*, 1500212.
[7] E. Peled, A. Gorenshtein, M. L. Sega, Y. Sternberg, *J. Power Sources* **1989**, *26*, 269–271.
[8] J. Hassoun, B. Scrosati, *Angew. Chem. Int. Ed.* **2010**, *49*, 2371–2374; *Angew. Chem.* **2010**, *122*, 2421–2424.
[9] L. F. Nazar, M. Cuisinier, Q. Pang, *MRS Bull.* **2014**, *39*, 436–442.
[10] R. D. Rauh, K. M. Abraham, G. F. Pearson, J. K. Surprenant, S. B. Brummer, *J. Electrochem. Soc.* **1979**, *126*, 523–527.
[11] N. Jayaprakash, J. Shen, S.-S. Moganty, A. Corona, L.-A. Archer, *Angew. Chem. Int. Ed.* **2011**, *50*, 5904–5908; *Angew. Chem.* **2011**, *123*, 6026–6030.
[12] D. Bresser, S. Passerini, B. Scrosati, *Chem. Commun.* **2013**, *49*, 10545–10562.
[13] M. Hagen, D. Hanselmann, K. Ahlbrecht, R. Maça, D. Gerber, J. Tübke, *Adv. Energy Mater.* **2015**, *5*, 1401986.
[14] R. Chen, T. Zhao, F. Wu, *Chem. Commun.* **2015**, *51*, 18–33.
[15] A. Manthiram, S.-H. Chung, C. Zu, *Adv. Mater.* **2015**, *27*, 1980–2006.
[16] F. Wu, J. Z. Chen, R. J. Chen, S. X. Wu, L. Li, S. Chen, T. Zhao, *J. Phys. Chem. C* **2011**, *115*, 6057–6063.
[17] C. Wang, W. Wan, J. T. Chen, H. H. Zhou, X. X. Zhang, L. X. Yuan, Y. H. Huang, *J. Mater. Chem. A* **2013**, *1*, 1716–1723.
[18] W. Y. Li, G. Y. Zheng, Y. Yang, Z. W. Seh, N. Liu, Y. Cui, *Proc. Natl. Acad. Sci. USA* **2013**, *110*, 7148–7153.
[19] Y. Z. Fu, A. Manthiram, *J. Phys. Chem. C* **2012**, *116*, 8910–8915.
[20] L. Wang, Z. H. Dong, D. Wang, F. X. Zhang, J. Jin, *Nano Lett.* **2013**, *13*, 6244–6250.
[21] H. Pan, X. Wei, W. A. Henderson, Y. Shao, J. Chen, P. Bhattacharya, J. Xiao, J. Liu, *Adv. Energy Mater.* **2015**, *5*, 1500113.
[22] R. Xu, J. Lu, K. Amine, *Adv. Energy Mater.* **2015**, *5*, 1500408.
[23] K. H. Wujcik, T. A. Pascal, C. D. Pemmaraju, D. Devaux, W. C. Stolte, N. P. Balsara, D. Prendergast, *Adv. Energy Mater.* **2015**, *5*, 1500285.
[24] C. Barchasz, F. Molton, C. Duboc, J.-C. Leprêtre, S. Patoux, F. Alloin, *Anal. Chem.* **2012**, *84*, 3973–3980.
[25] K. Amine, R. Kanno, Y. Tzeng, *MRS Bull.* **2014**, *39*, 395–401.
[26] R. Xu, I. Belharouak, J. C. M. Li, X. Zhang, I. Bloom, J. Bareño, *Adv. Energy Mater.* **2013**, *3*, 833.
[27] W. Li, Z. Liang, Z. Lu, H. Yao, Z. W. Seh, K. Yan, G. Zheng, Y. Cui, *Adv. Energy Mater.* **2015**, *5*, 1500211.
[28] R. Cao, W. Xu, D. Lv, J. Xiao, J.-G. Zhang, *Adv. Energy Mater.* **2015**, *5*, 1402273.
[29] S. Zhang, K. Ueno, K. Dokko, M. Watanabe, *Adv. Energy Mater.* **2015**, *5*, 1500117.
[30] S. Urbonaite, T. Poux, P. Novák, *Adv. Energy Mater.* **2015**, *5*, 1500118.
[31] M. Agostini, J. Hassoun, J. Liu, M. Jeong, H. Nara, T. Momma, T. Osaka, Y.-K. Sun, B. Scrosati, *ACS Appl. Mater. Interfaces* **2014**, *6*, 10924–10928.
[32] D. Aurbach, E. Pollak, R. Elazari, G. Salitra, C. S. Kelley, J. Affinito, *J. Electrochem. Soc.* **2009**, *156*, A694–A702.
[33] C. Barchasz, J.-C. Leprêtre, S. Patoux, F. Alloin, *Electrochim. Acta* **2013**, *89*, 737–743.
[34] M. Galiński, A. Lewandowski, I. Stępniak, *Electrochim. Acta* **2006**, *51*, 5567–5580.
[35] A. Lewandowski, A. Świderska-Mocek, *J. Power Sources* **2009**, *194*, 601–609.
[36] O. Borodin, G. D. Smith, O. Geiculescu, S. E. Creager, B. Hallac, D. DesMarteau, *J. Phys. Chem. B* **2006**, *110*, 24266–24274.
[37] W. L. Jorgensen, J. Tirado-Rives, *Proc. Natl. Acad. Sci. USA* **2005**, *102*, 6665–6670.
[38] W. L. Jorgensen, D. S. Maxwell, J. Tirado-Rives, *J. Am. Chem. Soc.* **1996**,*118*, 11225–11236.
[39] G. A. Kaminski, R. A. Friesner, J. Tirado-Rives, W. L. Jorgensen, *J. Phys. Chem. B* **2001**, *105*, 6474–6487.
[40] N. M. Fischer, P. J. Van Maaren, J. C. Ditz, A. Yildirim, D. van der Spoel, *J. Chem. Theory Comput.* **2015**, *11*, 2938–2944.
[41] H. J. C. Berendsen, D. van der Spoel, R. van Drunen, *Comp. Phys. Comm.* **1995**, *91*, 43–56.
[42] T. H. Dunning Jr., *J. Chem. Phys.* **1989**, *90*, 1007–1023.
[43] M. J. Frisch, G. W. Trucks, H. B. Schlegel, G. E. Scuseria, M. A. Robb, J. R. Cheeseman, G. Scalmani, V. Barone, G. A. Petersson, H. Nakatsuji et. Al. *Gaussian 09*, Revision D.01; Gaussian, Inc.: Wallingford, CT, **2009**.
[44] C. Caleman, P. J. van Maaren, M. Hong, J. S. Hub, L. T. Costa, D. van der Spoel, *J. Chem. Theory Comput.* **2012**, *8*, 61–74.
[45] T. Darden, D. York, L. Pedersen, *J. Chem. Phys.* **1993**, *98*, 10089–10092.
[46] M. Salanne, *Phys. Chem. Chem. Phys.* **2015**, *17*, 14270–14279.
[47] M. I. Chaudhari, J. R. Nair, L. R. Pratt, F. A. Soto, P. B. Balbuena, S. B. Rempe, *J. Chem. Theory Comput.* **2016**, *12*, 5709–5718.
[48] M. Salanne, R. Vuilleumier, P. A. Madden, C. Simon, P. Turq, B. Guillot, *J. Phys. Condens. Matter* **2008**, *20*, 494207.
[49] C. Wohlfarth in Lechner M. D. (eds) Optical Constants. Condensed Matter, vol 50., **2017**, Springer, Berlin, Heidelberg.
[50] K. Hayamizu, Y. Aihara, S. Arai, C. G. Martinez, *J. Phys. Chem. B* **1999**, *103*, 519–524.
[51] K. Hayamizu, Y. Aihara, *Electrochim. Acta* **2004**, *49*, 3397–3402.
[52] K. Hayamizu, E. Akiba, T. Bando, Y. Aihara, *J. Chem. Phys.* **2002**, *117*, 5929.
[53] J. N. Canongia Lopes, A. A. H. Pàdua, *J. Phys. Chem. B* **2004**, *108*, 16893–16898.
[54] O. Borodin, *J. Phys. Chem. B* **2009**, *113*, 11463–11478.
[55] D.-R. Chang, S.-H. Lee, S.-W. Kim, H.-T. Kim, *J. Power Sources* **2002**, *112*, 452–460.

Manuscript received: December 21, 2018
Revised manuscript received: February 1, 2019
Version of record online: February 14, 2019